Available online at www.sciencedirect.com
ScienceDirect
Journal of Molecular Catalysis A: Chemical 268 (2007) 176–184
JOURNAL OF MOLECULAR CATALYSIS A: CHEMICAL
www.elsevier.com/locate/molcata

# Cross-linked poly-4-vinylpyridines as useful supports in metal catalysis: micro- and nanometer scale morphology

Maria Giammatteo [a], Leonardo Tauro [b], Angelo A. D'Archivio [c,*], Luciano Galantini [d], Alberto Panatta [e], Enzo Tettamanti [f], Karel Jerabek [g,*], Benedetto Corain [h,*]

[a] *Centro di Microscopia Elettronica, Università di L'Aquila, Monteluco di Roio, 67040 L'Aquila, Italy*
[b] *Dipartimento di Mineralogia e Petrologia, Università di Padova, Corso Garibaldi 37, 35137 Padova, Italy*
[c] *Dipartimento di Chimica Ingegneria Chimica e Materiali, Università di L'Aquila, Via Vetoio, Coppito, 67010 L'Aquila, Italy*
[d] *Dipartimento di Chimica, Università di Roma "La Sapienza", P.le Aldo Moro 5, 00185 Roma, Italy*
[e] *Istituto Nazionale di Fisica della Materia (INFM), Dipartimento di Fisica, Università di L'Aquila, Via Vetoio, Coppito, 67010 L'Aquila, Italy*
[f] *Dipartimento di Scienze Biomediche Comparate, Università di Teramo, P.zzale A. Moro 45, 64100 Teramo, Italy*
[g] *Institute of Chemical Process Fundamentals, Rozvojova 135, CR-16502 Suchdol, Praha 6, Czech Republic*
[h] *Istituto di Scienze e Tecnologie Molecolari, C.N.R., Sezione di Padova c/o Dipartimento di Scienze Chimiche, Via Marzolo 1, 35131 Padova, Italy*

Received 3 August 2006; received in revised form 5 December 2006; accepted 6 December 2006
Available online 15 December 2006

**Abstract**

Three commercially available poly-4-vinylpyridine resins, two of gel-type (2% cross-linked) and one macroreticular in nature (25% cross-linked) are investigated in the solid state with SEM and in the swollen state with a combination of inverse steric exclusion chromatography (ISEC) and ESR (test of rotational mobility of the spin probe TEMPONE) in various liquid media. In all cases the materials result to be scarcely swellable but, after iodomethylation they develope a quite noticeable nanoporosity in methanol, water and water/methanol/acetic acid. These observations are particularly valuable in the case of the resin Reilex 425 (Reilly Industries, Inc., USA) that is, in its iodomethylated form, the support of $[Rh(CO)_2I_2]$-, i.e. the actual "molecular" catalyst in the innovative Chiyoda-UOP industrial synthesis of acetic acid (Acetica process).


*Keywords:* Cross-linked functional polymers; Poly-4-vinylpyridines; Supported Pt(0) nanoclusters; Chiyoda-UOP Acetica process; Support nanostructure; ISEC analysis

## 1. Introduction

Cross-linked functional polymers (CFPs), so far commonly named functional resins [1–2], have been (and are) considered as promising supports for metal catalysis for many years. In fact, seminal patents by Haag and Whitehurst [3] (Mobil Oil) put forward in 1969 the idea of employing CPFs as macro-ions and macro-ligands for supporting in the liquid phase metal species known to be catalytically active in homogeneous phase. To our knowledge, for these peculiar macromolecular complexes Grubbs coined the term "hybrid phase catalysts" in 1972 [4]. Interestingly, although the proposal promoted the production of thousands of papers and patents [5], the first relevant industrial application appeared only in 1998 (Chiyoda-UOP Acetica process [6]).

Year 1969 witnessed the appearance of another seminal patent by Wöllner and Neier, Bergbau Chemie [7], in which CFPs were proposed as supports of palladium metal to give $Pd^0$/CPF innovative bifunctional catalysts. These materials found immediate applications in the innovative one-pot synthesis of methyl-isobutylketone from acetone and dihydrogen, which was later followed by three other significant achievements [8].

Quite in contrast with the very alive interest caused by the idea of the hybrid phase catalysis, this second proposal met a very pale interest in academic and industrial communities [9–13] at least till the early nineties. In fact, we started in those years [8] a systematic development of practical protocols for the metallation of CFPs and for the generation of size-controlled metal

* Corresponding authors.
*E-mail addresses:* darchivi@univaq.it (A.A. D'Archivio), KJER@icpf.cas.cz (K. Jerabek), benedetto.corain@unipd.it (B. Corain).

1381-1169/$ – see front matter © 2006 Elsevier B.V. All rights reserved.
doi:10.1016/j.molcata.2006.12.014

nanoclusters inside their nanoporous domains [14–15]. Interestingly, in more recent years, also American [16], British [17–19], Japanese [20] and Chinese [21] groups have been effectively contributing to these topics.

In the frame of our endeavour towards promising $M^0$/CPF catalysts, we came across a commercially available macroligand and potential macromolecular support for nanoclustered metals, i.e. 2% cross-linked (with divinylbenzene) poly-4-vinylpyridine (Aldrich), hereafter coded as **CF4** [22–23].

Some very peculiar unpublished microstructural features of **CF4** observed in our recent studies, prompted us to carry out a thorough micro- and nanometer level characterization of both our **$Pt^0$/CF4** catalyst and of the support itself. Moreover, we have been also attracted by resin Reillex 402 (hereafter referred to as **R402**) (Reilly Corporation) 2% cross-linked and by Reillex 425 (hereafter referred to as **R425**) ca. 25% cross-linked and therefore expected to be macroreticular in nature. A possible similarity of the micro- and nanostructure of **CF4** and **R402** and *the relevance of **R425** to the support of* $[Rh(CO)_2I_2]$- *in the very innovative Acetica process* (*a new industrial way of access to acetic acid*), prompted us to include also these two materials (and their iodomethylated forms) in our investigation.

Our analysis is pivoted in the combined and critical employment of inverse steric exclusion chromatography (ISEC) (suitable to provide quantitative information on the nanoporosity of the swollen matrix) and of ESR spectroscopy (suitable to report on the rotational mobility of a given paramagnetic probe located inside of the nanoporous domains of the swollen material [24]).

## 2. Experimental

### 2.1. Chemicals and methods

Solvents and reagents were of reagent grade and were used as received. Commercial resin **CF4** from Aldrich was sieved to give 400 and 180 μm particles, **R402** and **R425** commercialized as sub-millimeter beads, were from Reilly Industries, Inc., USA and were used as received. The estimated cross-linking degree for **R402** is 2% and for **R425** 25%. Elemental analyses (%). **CF4**: C = 77.25; H = 6.06; N:12.62. **R402**: C = 75.66; H = 6.80; N:12.32. **R425**: C = 79.45; H = 6.79; N:8.54.

Iodomethylated **R402** and **R425** were obtained as follows: 10 g of the polymer were suspended in 10 $cm^3$ acetone. After 3 h of swelling, 10.7 $cm^3$ of methyl iodide were added and the mixture was kept at laboratory temperature with occasional stirring for 3 days (this stirring procedure was chosen in order to prevent the powdering of the resin beads that more energetic stirring procedure would have caused. On the other hands, in view of the longer contact time, it is estimated that diffusion problems of methyl iodide from the solution to the resin particles can be safely neglected in spite of the lack of vigorous stirring). Iodomethylated product was then separated, washed with deionized water and dried at 100 °C overnight. **R425MeI**, turns out to be thermally stable under nitrogen up to 220 °C (thermogravimetric analysis).

Elemental analyses. **R402MeI**: 3.66 meq/g (total iodine content). **R425MeI**: 3.16 meq/g (total iodine content).

Catalyst **$Pt^0$/CF4** was prepared with the Metal Vapour Synthesis protocol [22–23]. A suitable sample of **CF4** (typically 2 g) is let to be swollen in 20 ml mesitylene and let to interact with a proper amount of a standardized mesitylene solution of $Pt^0$ "solvated atoms" [25]. The dark brown suspension turns rapidly to a black one in which the solid phase is black and the surnatant liquid phase is in fact clear and colourless. Operations were set up to give a **$Pt^0$/resin** composite featured by ca. 1% metal.

### 2.2. SEM and TEM analysis

SEM pictures were taken with a CAMSCAN MX2500 apparatus. TEM pictures were taken with a Philips CM200 microscope. Ultrathin sections (nominal thickness 30 nm) were cut with a Leica ULTRACUT-R ultramicrotome.

### 2.3. Specific absorbed volume (SAV) measurements

The apparatus and procedures are illustrated in [26,27].

### 2.4. Inverse steric exclusion chromatography (ISEC)

$D_2O$, sugars and polydextranes in aqueous sodium sulphate solution (0.2 M) as the mobile phase, were employed as standard solutes in ISEC characterization of water-swollen resins. Organic solvent-swollen state was investigated using THF as the mobile phase and *n*-alkanes and polystyrenes as the standard solutes. Details of the experimental procedure and data treatment were reported elsewhere [28–31].

### 2.5. ESR analysis

The ESR spectra were recorded in the temperature range 10–45 °C at 5 degrees intervals, using an X-band JEOL JES-RE1X apparatus working at 9.2 GHz (modulation 100 kHz). During the measurements, the temperature of the sample was controlled with a variable temperature unit Steler VTC91, the accuracy being ±0.1 °C.

About 0.2 g of ground material was swollen with nitrogen-saturated $10^{-4}$ M solution of the paramagnetic probe TEMPONE in the required solvent. The sample was allowed to reach the swelling equilibrium, and after pouring the suspension onto filter paper to remove the excess solution, a suitable amount of swollen material was quickly transferred into the ESR tube.

The spectra of the spin probe generally appear as those typical of a fast-motional regime [32–34]. Under these conditions, the rotational correlation time $\tau$ of TEMPONE was calculated according to the formula [32–34].

$$\tau = 6.14 \times 10^{-10} \Delta H_0 \left[ \left( \frac{h_0}{h_{+1}} \right)^{1/2} + \left( \frac{h_0}{h_{-1}} \right)^{1/2} - 2 \right] \times \left[ 1 - \frac{1}{5(1 + \omega_e^2 \tau^2)} \right]$$

where $\omega_e = 5.78 \times 10^{-10}$ Hz; the parameters $h_{+1}$, $h_0$ and $h_{-1}$ (the intensities of the low-, middle- and high-field lines, respectively) and $\Delta H_0$ (the peak-to-peak width of the central line) were obtained by peak-picking from the first derivative spectrum. The numerical constant in s/G was evaluated by using the known values of the components of the hyperfine $A$ tensor observed in single crystal [35]: $A_x = 5.5$ G, $A_y = 5.8$ G, $A_z = 32.5$ G. To account for polarity effects, the right hand side of the above equation was multiplied by $(a_N/a_{iso})^2$, where $a_N = (A_x + A_y + A_z)/3$ and $a_{iso}$ is the hyperfine isotropic term evaluated from the observed splitting in motionally averaged spectra.

## 3. Results and discussion

### 3.1. SEM and TEM analysis

SEM pictures of **CF4** (Fig. 1) and of **R402** (Fig. 2) reveal a very unusual micromorphology for gel-type resins. Normal gel-type CFPs particles do exhibit in fact a glass-like appearance up to 5000 magnifications and *individual resins particles* are just single compact entities (*vide infra*).

**CF4** and **R402** are seen to be built up with sort of "minibeans" that are separated by relatively large "channels" and appearing as quite compact entities at the highest magnification. Quite in contrast with this pattern, SEM of **R425** (Fig. 3) reveals the classic macroporous structure of macroreticular CFPs.

As to **$Pt^0$/CF4** nanocomposite, SEM analysis of back-scattered electrons (Fig. 4a) and XRMA of Pt distribution through the section of a resin particle (Fig. 4b), suggest that $Pt^0$ nanoclusters are deposited at the external surface of the "minibeans" illustrated in Figs. 1 and 2.

Consequently, $Pt^0$ nanoclusters are expected to be seen, by low resolution TEM of thin sections of catalyst particle, as very elongated ribbons (Fig. 5).

### 3.2. Swelling behaviour: specific absorbed volume (SAV) analysis of *CF4* and *R402*

SAV analysis was proposed in 1952 [26] as a practical and somewhat accurate means for determining the solvent compatibility of a given CFP material. The swelling ability is assessed by weight determination of the solvent retention, after stripping of the occluded solvent by centrifugation [26–27]. The specific absorbed solvent volume (SAV) expresses quantitatively the mutual affinity of the resin and the solvent. Collected data are shown in Table 1 both for **CF4** and for **R402** (according to published manufacturer's data, **R402** should be very similar to **CF4**).

It is seen that **CF4** and **R402** are poorly swollen in a variety of diverse solvents, including methanol, which is a renown widely compatible swelling medium [36]. Notice that mesitylene, i.e. the medium in which the generation of $Pt^0$ nanoclusters onto **CF4** from the gas phase occurs [25] is by far the worse swelling agent. In spite of this, **$Pt^0$/CF4** assembled in mesitylene exhibits a respectable activity and chemoselectivity in the hydrogenation of citrale to geraniol and nerol [22] in ethanol and **$Pd^0$/CF4** also assembled in mesitylene represents one of the very few authentically heterogeneous Heck catalysts in *N*,*N*-dimethylacetamide and in 3-methyl-2-pyrrolidone [23] in which media SAV figures are also very small.

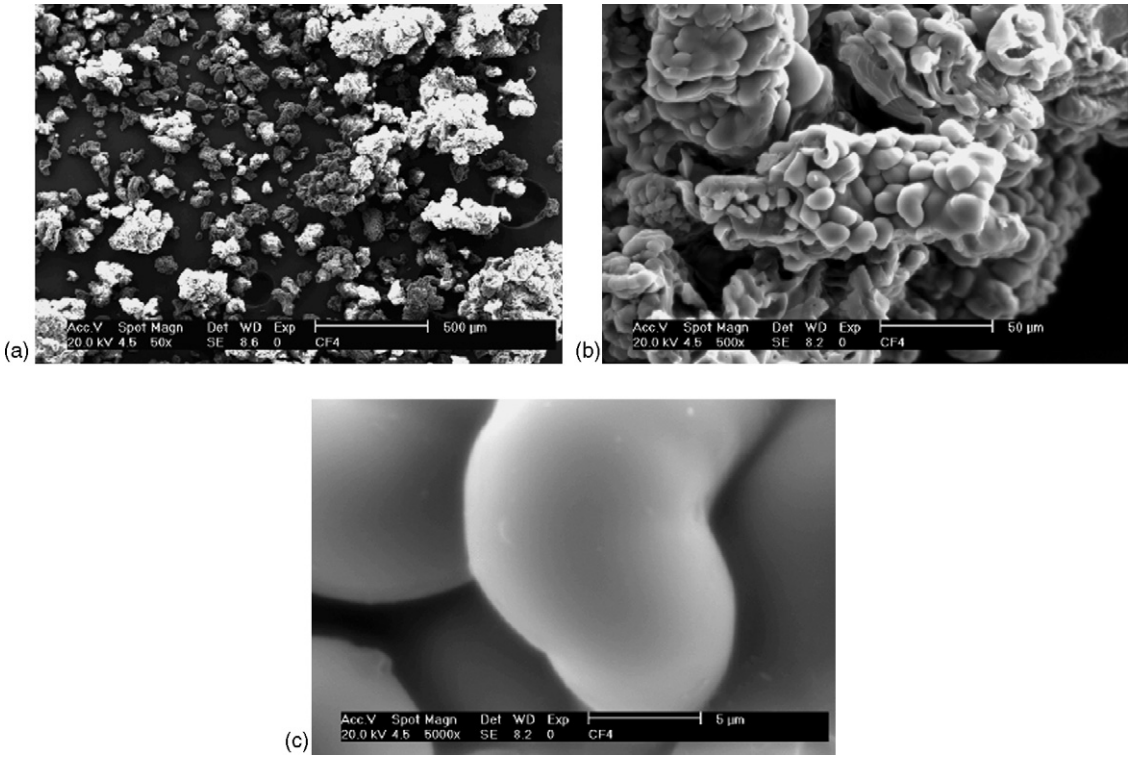


Fig. 1. SEM pictures of **CF4** at various magnifications.

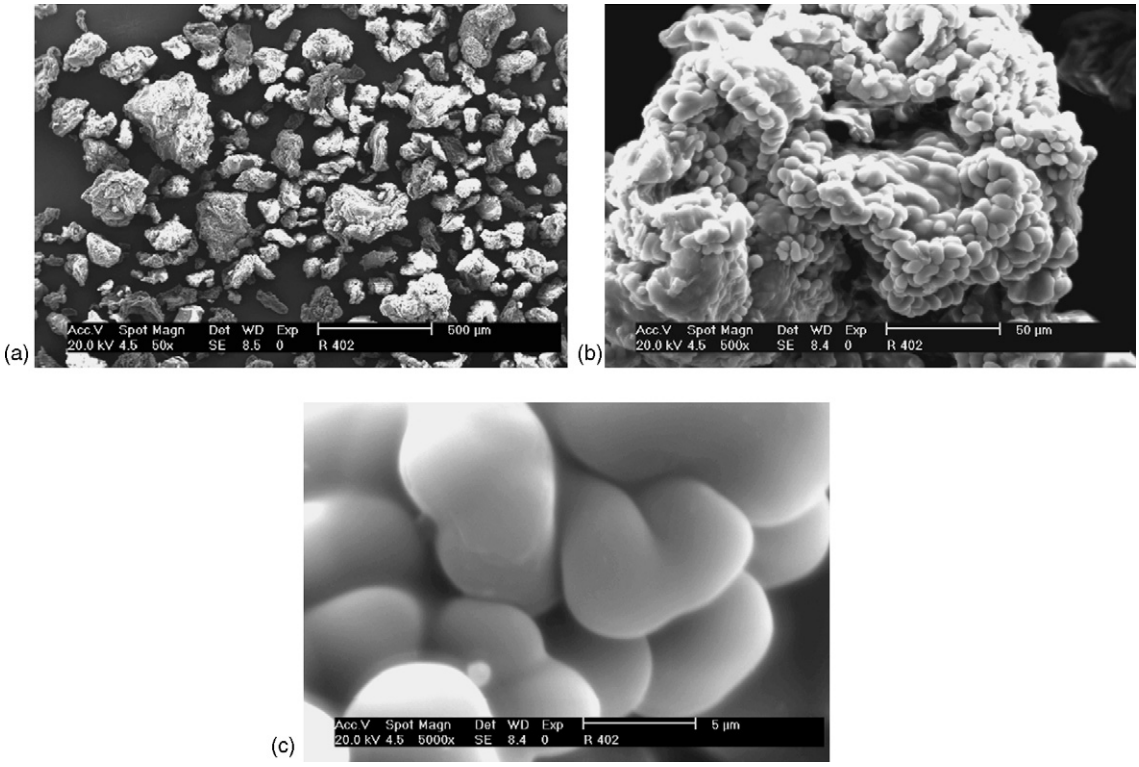


Fig. 2. SEM pictures of **R402** at various magnifications.

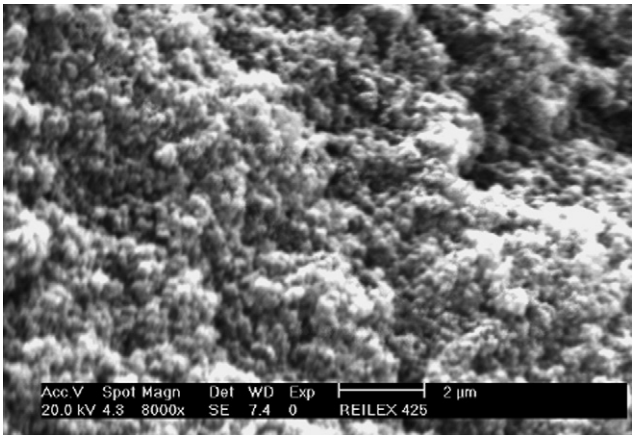


Fig. 3. SEM picture of **R425**.

Table 1
SAV values for various solvents inside **CF4** and **R402**

| Solvent | **R402** (ml/g) | **CF4** (ml/g) |
|---|---|---|
| Methanol | 1.10 | 1.18 |
| Ethanol | 1.11 | |
| Propanol | 1.00 | |
| *N*,*N*-dimethylformamide | 0.74 | |
| *N*,*N*-dimethylacetamide | 0.52 | 0.70 |
| Water | 0.51 | 0.56 |
| Acetonitrile | 0.51 | 0.46 |
| 3-Methyl-2-pirrolydone | 0.50 | |
| Tetrahydrofurane | 0.37 | 0.57 |
| Dioxane | 0.19 | |
| *n*-Pentane | 0.18 | |
| Mesytilene | | 0.21 |
| 1,2-Dichloroethane | | 0.76 |

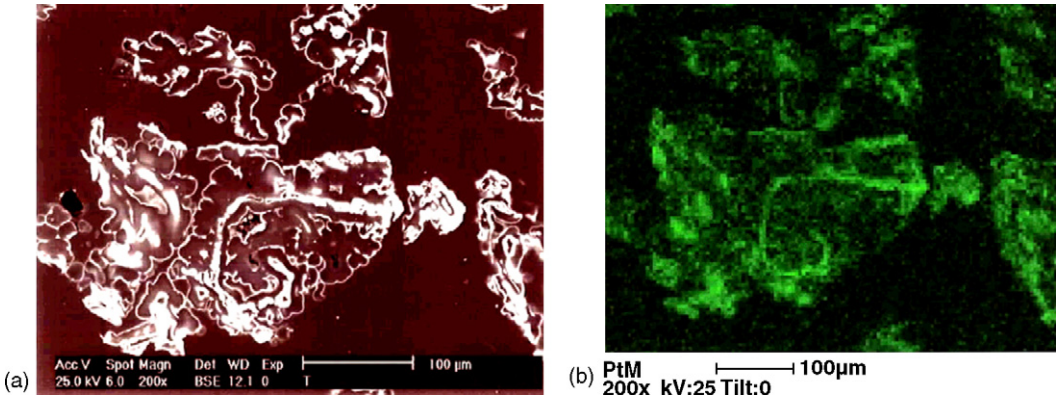


Fig. 4. SEM analysis of back-scattered electrons (a) and XRMA of Pt distribution on the same section (b) of **$Pt^0$/CF4**.

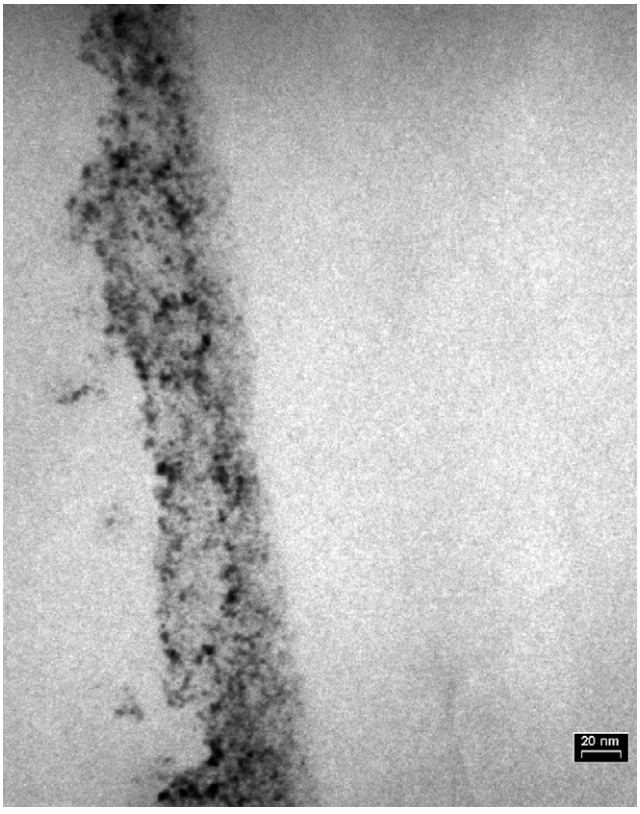


Fig. 5. TEM picture of a ca. 400 nm thick section of a **$Pt^0$/CF4** catalyst particle showing a typical ribbon made of $Pt^0$ nanoclusters (bar = 10 nm). The ribbon is believed to be formed by the metal nanoclusters laying outside one of the "minibeans" that build up the entire structure of a resin particle (see Fig. 1).

As a final comment of the data of this paragraph, we stress the circumstance that the observed scarce swellability of both **CF4** and **R402** in such numerous and diverse solvents is a really a surprising finding for the usual lightly cross-linked CFPs. Indeed, in the frame of our wide experience, a 2% cross-linked gel-type resin with such a reluctance to swelling is an unprecedented observation. Apparently some sort of extensive inter-chain non-covalent interaction has to take place.

### *3.3. Nanostructure of **CF4**, **R402**, **R425**, **R402MeI**, **R425MeI**: assessment with ISEC*

ISEC provides detailed information on the swollen-state morphology of crosslinked polymers [28–31]. It is based on the analysis of the elution behaviour of standard solutes with known effective molecular size flowing through a column filled with the investigated material under conditions where the chromatographic process is influenced by steric (entropic) effects only. Similarly to the case of the other porosimetric methods, the mathematical treatment of the elution data is based on depicting of the morphology of the investigated material using a simple geometrical model. It has been proven that the morphology of swollen polymer gels is best described on the basis of the so called Ogston's model [37] that depicts pores as spaces among randomly oriented rigid rods. This simplified depiction of the morphology of swollen polymer networks provides a fair description of both the intensive parameters (polymer chain densities) and extensive properties (specific volumes of variously dense polymer fractions). On the other hand, the basic character of the much more common cylindrical pore model depicting pores as cylindrical holes in a solid matter differs from the physical reality of the polymer framework geometry rather substantially. However, although the description of the swollen morphology of a polymer matrix based on the cylindrical pore model produces unrealistic values for the *pores volumes* (extensive properties), it provides a useful description of the porosity in terms of *pores diameter* distribution (intensive property), i.e. a quantity more easily feasible than the polymer chain density.

Table 2
Nanometer scale morphology of **R425** swollen in THF as revealed by ISEC

| Macropores | |
|---|---|
| Pore diameter (nm) | Pore volume ($cm^3/g$) |
| 42.9 | 0.687 |
| 81.8 | 0.047 |
| 234.5 | 0.054 |
| Sum | 0.788 |
| **Swollen polymer gel** | |
| Polymer chain concentration ($nm/nm^3$) | Polymer fraction volume ($cm^3/g$) |
| 0.1 | 0 |
| 0.2 | 0 |
| 0.4 | 0 |
| 0.8 | 0 |
| 1.5 | 0.394 |
| Sum | 0.394 |

Attempts to characterize **CF4**, **R402** and **R425** by ISEC in water, were unsuccessful due to the insufficient swelling of the polymer framework and to adsorption of some dextranes on the walls of macropores in **R425**. Even in THF resins **CF4** and **R402** are little penetrable materials with practically no measurable porosity. **R425** exhibits in THF a very modest swollen polymer gel volume while its macropores appear well evident (see Table 2).

Quaternization of the pyridine groups in these polymers by iodomethylation dramatically changes their swelling behavior. The iodomethylated **R402** (**R402MeI**) is seen to swell quite extensively in water (Table 3) while in THF its swelling remains negligible.

Table 3
Nanometer scale morphology of **R402MeI** swollen in water as revealed by ISEC

| Polymer chain concentration ($nm/nm^3$) | Polymer fraction volume ($cm^3/g$) |
|---|---|
| 0.1 | 0.037 |
| 0.2 | 0.000 |
| 0.4 | 0.527 |
| 0.8 | 0.313 |
| 1.5 | 0.831 |
| Sum | 1.708 |

Table 4
Nanometer scale morphology of **R425MeI** swollen in water and THF as revealed by ISEC

| Macropores | | | |
|---|---|---|---|
| Water | | THF | |
| Pore diameter (nm) | Pore volume ($cm^3/g$) | Pore diameter (nm) | Pore volume ($cm^3/g$) |
| 14.5 | 0.328 | 9.4 | 0.036 |
| 20.1 | 0.028 | 12.9 | 0.020 |
| 32.6 | 0.230 | 45.8 | 0.067 |
| | | 70.5 | 0.258 |
| Sum | 0.586 | Sum | 0.381 |

| Swollen polymer gel | | | |
|---|---|---|---|
| Water | | THF | |
| Swollen polymer gel polymer chain concentration ($nm/nm^3$) | Polymer fraction volume ($cm^3/g$) | Polymer chain concentration ($nm/nm^3$) | Polymer fraction volume ($cm^3/g$) |
| 0.1 | 0.004 | 0.1 | 0.000 |
| 0.2 | 0.019 | 0.2 | 0.000 |
| 0.4 | 0.000 | 0.4 | 0.000 |
| 0.8 | 0.000 | 0.8 | 0.000 |
| 1.5 | 0.535 | 1.5 | 0.017 |
| Sum | 0.558 | Sum | 0.017 |

Also **R425MeI** is found to swell much better in water than in THF (Table 4).

As it was already mentioned above, depicting the swollen polymer mass as arrays of polymer chains featured by given polymer chains concentrations provides a reasonable, physically ground image of the polymer framework, but it does not permit a straight estimate of the size and distribution of cavities inside the three-dimensions mesh system. For such assessment we have often successfully employed [14] the conventional model of cylindrical pores (Table 5).

It is quite apparent that the quaternization of **R402** and of **R425** produces a great increase of the interaction of the polymer chains with water as solvent resulting in a relatively large swelling and increase of the nanoporosity (and consequently of molecular accessibility of the polymer frameworks). The availability after iodomethylation of 1.11 $cm^3$ of swollen polymer gel in water-swollen **R425MeI** per gram of resin, militates in favour of the circumstance that $[Rh(CO)_2I_2]$- units located at the "macropores surface" [38] should be reasonably accessible to CO, MeOH and MeI, reagents and co-catalyst, respectively, in the catalytic process.

This specific finding is conceptually very valuable for granting the Acetica-UOP catalyst the term "hybrid phase catalyst" and it is *the first industrially relevant "hybrid phase catalyst" since the time of Haag and Whitehurst's prophetic proposal* [3,5].

### *3.4. Rotational mobility of TEMPONE (2,2,6,6-tetramethyl-4-oxo-1-oxyl-piperidine) inside the nanoporous domains of **CF4**, **R402**, **R425**, **R402MeI**, **R425MeI***

The rotational mobility of a molecular probe such as TEMPONE or $Cu^{2+}$ complexes dissolved in a given medium let to swell a given CFP, is a practical and subtle tool for a quantitative estimate of the molecular accessibility and nanomorphology of gel-type resins [24,39,40].

In the case of **CF4**, in all investigated media the spin-probe is featured by a three-line ESR spectrum, typical of "fast-motional" reorientation, the correlation time of which (Table 6 and Fig. 6) can be obtained by line-shape analysis (see Section 2).

With the remarkable exception of mesitylene, in all other swelling media TEMPONE appears to be able to penetrate the

Table 5
Distribution of effective sizes of nanopores detected with ISEC analysis in the examined resins after swelling in water and THF

| Equivalent cylindrical pore diameter (nm) | Equivalent pore volume ($cm^3/g$) | | | |
|---|---|---|---|---|
| | **R425** THF | **R402MeI** Water | **R425MeI** Water | **R425MeI** THF |
| 12 | 0 | 0.06 | 0 | 0 |
| 8 | 0.02 | 0 | 0 | 0 |
| 4 | 0 | 0.35 | 0.06 | 0 |
| 2 | 0.05 | 0.95 | 0.19 | 0 |
| 1 | 0.52 | 0 | 0 | 0.05 |
| 0.5 | 0 | 1.25 | 1.06 | 0 |

Table 6
Rotational correlation times $\tau$ at 25 °C, apparent activation energies $E_a$ of rotational diffusion of TEMPONE in various media both in the bulk state (left column) and in the confined state (i.e. inside swollen **CF4** (right column))

| Medium | $\tau$ (ps) ± 5% | | $E_a$ (kJ/mol) | |
|---|---|---|---|---|
| Ethanol | 21 | 270 | 13.3 ± 0.5 | 9.5 ± 0.5 |
| Acetonitrile | 14 | 322 | 8 ± 1 | 16.8 ± 0.5 |
| Mesitylene | 24 | 30 | 8 ± 1 | 6 ± 1 |
| *N*,*N*-dimethylacetamide | 23 | 224 | 8 ± 1 | 7.7 ± 0.5 |
| 3-Methyl-2-pyrrolidone | 17 | 129 | 15.3 ± 0.5 | 3 ± 1 |

polymer framework, *at least to some extent*, as revealed by the expected appreciable decrease of the rotational mobility (an increase of $\tau$ (Table 6) of the spin probe [39,40].

Additional information on polymer morphology is based on the temperature dependence of spin-probe rotational diffusion, as quantified by the apparent activation energy ($E_a$) given by the Arrhenius plot of $\tau$ data. The invariance or a little increase of $E_a$, as compared with the value observed in the bulk medium, generally occurs in relatively accessible and homogenous CFPs [39,40], in which the spin-probe diffusion mechanism closely reflects that occurring in pure liquid. On the other hand, a substantial decrease of $E_a$ was found to be diagnostic of a some heterogeneity in the polymer morphology [34,24]. In this circumstance, the ESR line-shape is in fact affected by both rotational diffusion of the spin-probes located inside different kinds of nanodomains and exchange dynamics between these sites. This does seem to be the case of **CF4** in ethanol and 3-methyl-2-pyrrolidone, as also confirmed by the observed temperature behaviour of solvent diffusion (Pulse Gradient Spin Echo-NMR data [41].

Only in mesitylene, the substantial invariance of $\tau$ and $E_a$ seen for TEMPONE rotating in bulk and confined liquid militates in favour of the total inability of the spin probe to penetrate the polymer framework of **CF4**.

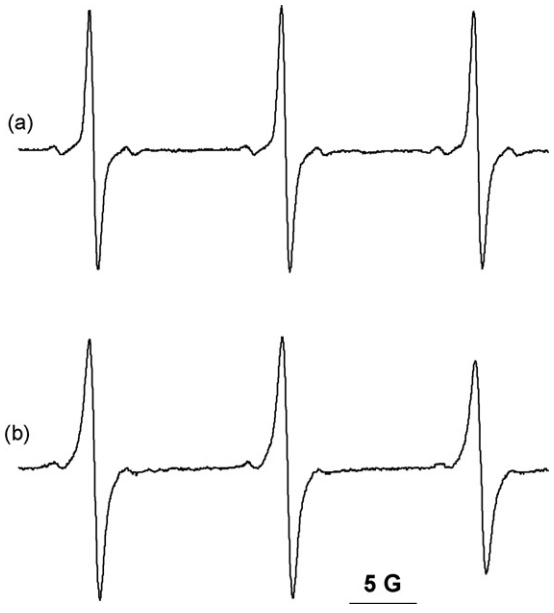


Fig. 6. ESR spectrum of TEMPONE rotating in bulk (a) and in **CF4**-confined (b) 3-methyl-2-pyrrolidone at 25 °C.

Table 7
Rotational correlation times $\tau$ at 25 °C, apparent activation energies $E_a$ of rotational diffusion of TEMPONE in various media both in the bulk state and in the confined state (i.e. inside swollen **R402**, **R402MeI**, **R425** and **R425MeI**)

| Medium | $\tau$ (ps) ± 5% | $E_a$ (kJ/mol) |
|---|---|---|
| Methanol | | |
| Bulk | 17 | 9.5 ± 0.5 |
| **R402** | 183 | 18.7 ± 0.5 |
| **R425** | 182 | 14.0 ± 0.5 |
| Acetonitrile | | |
| Bulk | 14 | 8 ± 1 |
| **R402** | 290 | 17 ± 1 |
| **R425** | 208 | 0 |
| THF | | |
| Bulk | 23 | 10 ± 1 |
| **R402** | 147 | Non-linear Arrhenius plot |
| **R402MeI** | 32 | 10 ± 1 |
| **R425** | 181 | Non-linear Arrhenius plot |
| **R425MeI** | 112 | 0 |
| Water | | |
| Bulk | 11 | 17.8 ± 0.5 |
| **R402** | 23 | Complicated line-shape above 40 °C |
| **R402MeI** | 30 | Complicated line-shape above 40 °C |
| **R425** | Bimodal spectrum | |
| **R425MeI** | 41 | 2 ± 0.5 |
| AcH–MeOH–$H_2O$ | | |
| Bulk | 21 | 10 ± 1 |
| **R402** | 74 | 0 |
| **R402MeI** | 38 | 0 |
| **R425** | 45 | 0 |
| **R425MeI** | 45 | 11 ± 1 |

The rotational mobility pattern of TEMPONE dissolved in methanol, acetonitrile, THF, water and in AcH–MeOH–$H_2O$ (50:45:5 mol), after permeation of **R402**, **R402MeI**, **R425**, **R425MeI**, is also somewhat complex (Table 7).

In fact, in addition to anomalous temperature behaviour (non-linear Arrhenius trends or very low $E_a$ values) observed in most of the cases, the ESR spectrum clearly exhibits a complex line-shape when water solution of TEMPONE permeates **R402** and **R402MeI** (above 40 °C) or **R425**. As an example, the spectrum of **R402MeI** at 45 °C, featured by an evident distortion of the high-field line, is given in Fig. 7a. As to **R425** in water, two spectral contributions are easily recognisable in the spectrum (Fig. 7b), which definitely supports the dispersion of the spin-probe in quite different environments [24].

On the basis of the above, one should take into account that also uncomplicated cases (apparent "fast-motion" spectra), may hide a complex spin-probe dynamics. However, even in this circumstance, $\tau$ provided by line-shape analysis still remains a suitable parameter for comparative evaluation of accessibility of the investigated materials and the swelling ability of the different media.

As a matter of fact, the behaviour of TEMPONE in **R402** and **R425** swollen in methanol, acetonitrile and THF is

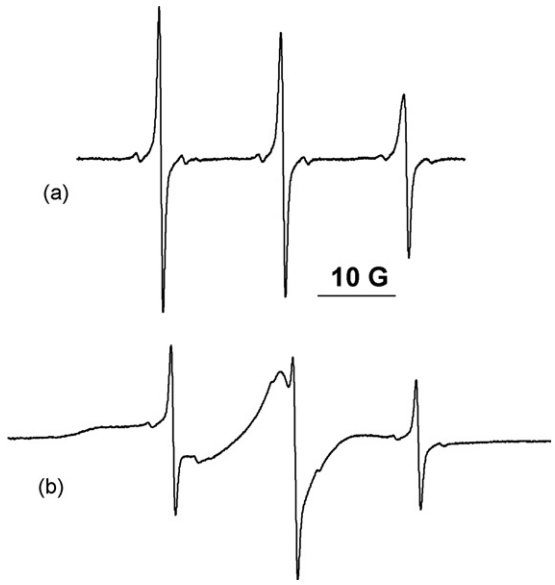


Fig. 7. ESR spectrum of a water solution of TEMPONE let to permeate **R402MeI** at 45 °C (a) or **R425** at 25 °C (b).

quite reminiscent of that seen in **CF4** (Table 6). TEMPONE rotates relatively slowly inside scarcely swollen frameworks that are consequently featured by smaller nanopores (higher $\tau$ values).

The behaviour of TEMPONE in **R402** and **R425** swollen in the AcH–MeOH–$H_2O$ mixture is quite similar to that observed in the other three media, but the swelling ability of the mixture is apparently better as witnessed by the smaller increase of $\tau$ values with respect to those observed in the bulk case.

The complexity of ESR spectra in water seems to reflect a certain heterogeneity of the polymer morphology. In the case of **R425** (Fig. 7b), the ESR line-shape clearly exhibits the coexistence of a "fast-motion" signal with a broad spectral ("slow-motion") component that has to be attributed to the partial immobilization of a significant fraction of TEMPONE molecules. Such immobilization can be due to the confinement of TEMPONE in small nanopores, as those revealed by ISEC, but adsorption of the spin-probe to the polymer framework cannot be excluded.

Quaternization does moderately affect the accessibility of **R402** in water and **R425** in AcH–MeOH–$H_2O$, while a significant increase of spin-probe mobility is detected for **R402** in AcH–MeOH–$H_2O$ and **R425** in THF or in water. In this last case, TEMPONE is in fact no more immobilized after iodomethylation of the polymer framework. These evidences are consistent with the general picture provided by ISEC analysis. An odd behaviour is that of **R402** in THF, for which quaternization induces a remarkable decrease of permeability of the polymer framework. The case of **R402MeI** swollen in THF is in fact probably similar to that of **CF4** in mesitylene (Table 6). Also in this case the macromolecular framework is so reluctant to swelling that TEMPONE turns out to be located only in a tiny external layer of THF so that the observed signal is just that provided by TEMPONE in bulk THF (*vide infra*).

## 4. Conclusion

Gel-type resins **CF4** and **R402** appear to exhibit an exceptionally low swellability in common solvents such as water, THF, n-alkanes, in spite of their low cross-linking degree (2%). Macroreticular resin **R425** exhibits a very modest swellability in THF, ca. 0.4 $cm^3\ g^{-1}$. After iodomethylation, both **R402** and **R425** exhibit a marked increase of swellability, a well measurable nanoporosity and in general a satisfactory molecular accessibility in water, methanol and water/methanol/acetic acid mixtures. These observations are pivotal in the rationalization of the satisfactory catalytic activity exhibited by the Chiyoda-UOP catalyst **R425Me$^+$[Rh(CO)$_2$I$_2$]$^-$**, i.e. the protagonist of the novel Acetica process.

## Acknowledgements

This work was partially supported by P.R.I.N. funding 2001–2003, Ministero dell'Università e della Ricerca Scientifica, Italy (project number 2001038991). We thank Prof. C. Corvaja, Dipartimento di Scienze Chimiche, for helpful discussion and for providing technical assistance in some ESR measurements.

## References

[1] A. Guyot, in: D.C. Sherrington, P. Hodge (Eds.), Synthesis and Separations using Functional Polymers, Wiley, New York, 1988, pp. 1–42.
[2] IUPAC Recommendation, Macromolecular Division-Sub-Committee on Macromolecular Terminology, 2004.
[3] W.O. Haag, D.D. Whitehurst, German Patents 1,800,371 (1969), 1,800,379 (1969), 1,800,380 (1969).
[4] R.H. Grubbs, CHEMTECH 7 (1977) 512–518.
[5] For a recent review paper, see: B. Corain, P. Centomo, M. Zecca, Chim. Ind. (Milan) 86 (2004) 114–121.
[6] N. Yoneda, S. Kusano, M. Yasui, P. Pujado, S. Wilcher, Appl. Catal. A: Gen. 221 (2001) 253–265.
[7] J. Wöllner, W. Neier, German Patent 1,260,454 (1969).
[8] B. Corain, P. Centomo, S. Lora, M. Kralik, J. Mol. Catal. A: Chem. 204–205 (2003) 755–762, and references therein (review paper).
[9] D.L. Hanson, J.R. Katzer, B.C. Gates, G.C.A. Schuit, J. Catal. 32 (1974) 204–215.
[10] J. Sabadie, J.-E. Germain, Bull. Chem. Soc. France (1974) 1133–1136.
[11] N.-H. Li, J.M.J. Frechet, J. Chem. Soc. Chem. Commun. (1985) 1100–1101.
[12] K. Jerabek, J. Mol. Catal. 55 (1989) 247–255.
[13] Among the various contributions of Toshima's group in Japan in the early nineties, see for example: Ohtaki, M. Komiyama, H. Hirai, N. Toshima, Macromolecules 24 (1991) 5567–5572.
[14] B. Corain, K. Jerabek, P. Centomo, P. Canton, Angew. Chem. Int. Ed. 43 (2004) 959–962.
[15] P.C. Burato, G. Pace, M. Favaro, L. Prati, B. Corain, J. Mol. Catal. A: Chem. 238 (2005) 26–34.
[16] S.N. Sidorov, I.V. Volkov, V.A. Davankov, M.P. Tsyurupa, P.M. Valetsky, L.M. Bronstein, R. Karlinsey, J.W. Zwanziger, V.G. Matveeva, E.M. Sulman, N.V. Lakina, E.A. Wilder, R.J. Spontak, J. Am. Chem. Soc. 123 (2001) 10502–10510.
[17] C. Ramarao, S.V. Ley, S.C. Smith, I.M. Shirley, N. DeAlmeida, Chem. Commun. (2002) 1132–1133.
[18] J.-Q. Yu, H.-C. Wu, C. Ramarao, J.B. Spencer, S. Ley, Chem. Commun. (2003) 678–679.
[19] V. Ley, C. Mitchell, D. Pears, C. Ramarao, J.-Q. Yu, W. Zhou, Org. Lett. (2003) 4665–4668.

[20] (a) N. Toshima, Y. Shiraishi, T. Teranishi, J. Mol. Catal. A: Chem. 177 (2001) 139–147;
(b) Y. Uozumi, R. Nakao, Angew. Chem. Int. Ed. 42 (2003) 194–197.
[21] F. Shi, Y. Deng, J. Catal. 211 (2002) 548–551.
[22] P. Centomo, S. Lora, M. Zecca, G. Vitulli, A.M. Caporusso, S. Galvagno, C. Milone, B. Corain, J. Catal. 229 (2005) 283–297.
[23] A.M. Caporusso, P. Innocenti, L.A. Aronica, G. Vitulli, R. Gallina, A. Biffis, M. Zecca, B. Corain, J. Catal. 234 (2005) 1–13.
[24] For a quite recent example of this approach, see: F. Pozzar, A. Sassi, G. Pace, S. Lora, A.A. D'Archivio, K. Jerabek, A. Grassi, B. Corain, Chem. Eur. J. 11 (2005) 7395–7404, and references therein.
[25] G. Vitulli, M. Bernini, S. Bertozzi, E. Pitzalis, P. Salvadori, S. Coluccia, G. Martra, Chem. Mater. 14 (2002) 1183–1186, and references therein.
[26] K.W. Pepper, D. Reichenberg, D.K. Hale, J. Chem. Soc. (1952) 3129–3136.
[27] J. Stamberg, S. Sevcik, Collect. Czech. Chem. Commun. 31 (1966) 1009.
[28] K. Jerabek, Anal. Chem. 57 (1985) 1595–1597.
[29] K. Jerabek, Anal. Chem. 57 (1985) 1598–1602.
[30] K. Jerabek, K. Setinek, J. Polym. Sci. Part A; Polym. Chem. Ed. 28 (1990) 1387–2395.
[31] K. Jerabek, in: M. Potschka, P.L. Dubin (Eds.), Cross Evaluation of Strategies in Size-Exclusion Chromatography, ACS Symposium Series 635, American Chemical Society, Washington, DC, 1996, pp. 211–224.
[32] P.L. Nordio, in: L.J. Berliner (Ed.), Spin Labeling, Theory and Applications, vol. I, Academic Press, New York, 1976, pp. 5–52.
[33] B.D. Chestnut, J.F. Hower, J. Phys. Chem. 75 (1971) 907–912.
[34] M.F. Ottavini, J. Phys. Chem. 91 (1987) 779–784.
[35] M. Brustolon, A.L. Maniero, C. Corvaja, Mol. Phys. 51 (1984) 1269–1281.
[36] R. Arshady, Adv. Mater. 3 (2001) 182–190.
[37] G. Ogston, Trans. Faraday Soc. (1958) 1754–1757.
[38] A.A. D'Archivio, L. Galantini, E. Tettamanti, A. Panatta, B. Corain, J. Mol. Catal. A: Chem. 157 (2000) 269–273.
[39] (a) T. Watanabe, T. Yahagi, S. Fujiwara, J. Am. Chem. Soc. 102 (1980) 5187–5191;
(b) D. Suryanarayana, P.A. Narayana, L. Kevan, Inorg. Chem. 22 (1983) 474–478;
(c) G.C. Rex, S. Schlick, J. Phys. Chem. 89 (1985) 3598–3601;
(d) C.G. Pitt, J. Wang, S.S. Shah, R. Sik, C.F. Chignell, Macromolecules 26 (1993) 2159–2164.
[40] (a) A. Biffis, B. Corain, M. Zecca, C. Corvaja, K. Jerabek, J. Am. Chem. Soc. 117 (1995) 1603–1606;
(b) A.A. D'Archivio, L. Galantini, A. Panatta, E. Tettamanti, B. Corain, J. Phys. Chem. B 102 (1998) 6774–6779.
[41] L. Galantini, unpublished results.